Dalton Transactions

PAPER

View Article Online
View Journal | View Issue

Cite this: *Dalton Trans.*, 2014, **43**, 9529

A highly selective and sensitive turn-on chemodosimeter for hypochlorous acid based on an iridium(III) complex and its application to bioimaging†

Fengniu Lu[a] and Tatsuya Nabeshima*[a,b]

Received 28th February 2014,
Accepted 10th April 2014

DOI: 10.1039/c4dt00616j

www.rsc.org/dalton

A novel and easily accessible luminescent iridium(III) complex $[Ir(tpy)_2(N^N)]PF_6$ (**Ir-ANMM**, tpy = 2-(*p*-tolyl)pyridine, N^N = 4-[(4-amino-3-nitrophenoxy)-methylene]-4′-methyl-2,2′-bipyridine) for the sensing of HOCl has been designed and synthesized. The detection strategy is based on the HOCl-promoted cleavage of the PET quenching 4-amino-3-nitrophenyloxy moiety of the weakly emissive complex **Ir-ANMM**, which gives rise to a highly luminescent complex $[Ir(tpy)_2(N^N')]PF_6$ (**Ir-HM**, N^N′ = 4-hydroxymethyl-4′-methyl-2,2′-bipyridine). Comparisons of the absorption, emission and mass spectra of **Ir-ANMM** in the absence and presence of HOCl have all confirmed the transformation of **Ir-ANMM** to **Ir-HM**. Titration and competition experiments have revealed high sensitivity and high selectivity of **Ir-ANMM** for HOCl, respectively. Significantly, the feasibility of the sensor under physiological conditions enables the successful luminescent imaging of HOCl in HeLa cells.

Introduction

Hypochlorous acid (HOCl) is a reactive oxygen species (ROS) and is widely employed in our daily lives as a bactericide and a bleaching agent.[1] As a normal byproduct of cellular metabolism,[2] endogenous HOCl plays essential roles in many vital biological processes. However, concentrated hypochlorite solutions can pose a great threat to health because excessive HOCl may result in tissue damage and numerous diseases.[3] The contribution of HOCl to both health and disease has strongly promoted the monitoring of HOCl and elucidation of its functional mechanisms both *in vivo* and *in vitro*. Many fluorescent sensors for HOCl have been reported in recent years.[4] However, such organic fluorophore-based sensors always suffer from a small Stokes shift and severe photobleaching.[5] Conversely, luminescent iridium(III) complexes exhibit advantageous photophysical properties such as good photostability, a large Stokes shift, high emission efficiency and sensitive optical properties to the chemical environment.[6] Consequently, a number of iridium(III) complexes have been employed as luminophores for sensing various analytes.[7]

Despite the significance of HOCl sensing and the attractive photophysical characteristics of iridium(III) complexes, there has been only one example of a hypochlorite sensor based on an iridium complex reported thus far.[8] The sensor, taking advantage of the oxidation of oxime, was capable of detecting hypochlorite. However, it suffers from poor water solubility due to the instability of oxime in aqueous media, which has undoubtedly limited its practical application. As a result, there remains a high demand for the development of practically applicable HOCl sensors based on the favorable iridium(III) complexes.

Recently, the reaction between the *o*-nitroanilino group and HOCl[9] has been successfully employed for the selective detection of HOCl.[10] Based on this reaction, we designed and synthesized an easily accessible chemodosimeter **Ir-ANMM** substituted with an *o*-nitroanilino group for HOCl sensing (Scheme 1). The sensor **Ir-ANMM** should possess very weak or no emission with the PET effect imposed by the electron-rich *o*-nitroanilino group. However, in the presence of HOCl, the *o*-nitroanilino group could be oxidized, followed by the cleavage of the 4-amino-3-nitrophenyloxy moiety and generation of a hydroxymethyl group appended complex **Ir-HM**, which, without the PET effect, should exhibit strong luminescence. Such a turn-on emission response can be well utilized for the sensing of HOCl. With an amino group and a hydroxyl group, respectively, both **Ir-ANMM** and **Ir-HM** should possess appro-

[a]*Graduate School of Pure and Applied Sciences, University of Tsukuba, Tsukuba, Ibaraki 305-8571, Japan. E-mail: nabesima@chem.tsukuba.ac.jp; Fax: +81-29-853-4507; Tel: +81-29-853-4507*
[b]*Tsukuba Research Center for Interdisciplinary Materials Science (TIMS), University of Tsukuba, Tsukuba, Ibaraki 305-8571, Japan*
†Electronic supplementary information (ESI) available. See DOI: 10.1039/c4dt00616j

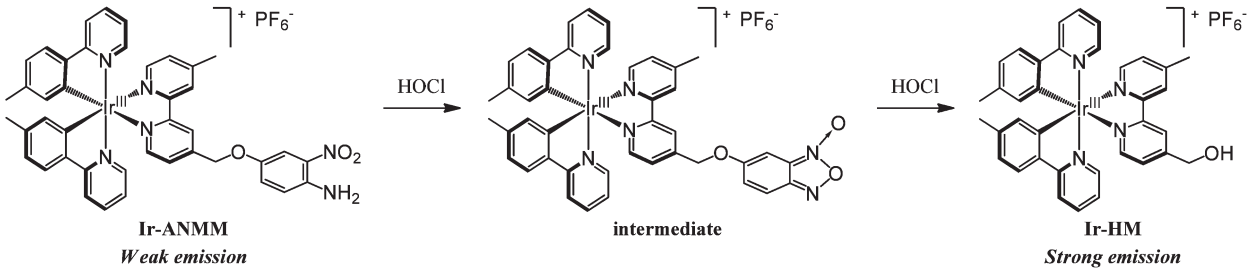

Scheme 1 The design concept of **Ir-ANMM**.

priate water solubility, enabling the detection of HOCl in aqueous media, which is a prerequisite of the sensor for practical applications. Moreover, a reaction-based chemodosimeter such as **Ir-ANMM** should possess very high selectivity.[11]

As anticipated, in the presence of HOCl, the weak emission of **Ir-ANMM** was remarkably enhanced. The absorption, emission and ESI mass spectral comparisons of **Ir-ANMM** in the absence and presence of HOCl have all confirmed the transformation of **Ir-ANMM** to **Ir-HM**. Significantly, the titration experiments indicated an extremely low detection limit, and the competition experiments demonstrated a highly specific luminescent response to HOCl among various reactive oxygen species (ROS) and reactive nitrogen species (RNS). These properties, together with the applicability of the sensing under physiological conditions, make **Ir-ANMM** capable of imaging HOCl in living cells, which is of striking importance for intracellular HOCl sensing in view of the significant biological impact of HOCl.

Experimental section

Materials

All starting materials and reagents, unless otherwise specified, were purchased from commercial suppliers and used without further purification. 4-Bromomethyl-4′-methyl-2,2′-bipyridine (**BM-bpy**),[12] 4-hydroxymethyl-4′-methyl-2,2′-bipyridine (**HM-bpy**),[13] and $[\mathbf{Ir(tpy)_2Cl}]_2$ [14] (tpy = 2-(*p*-tolyl)pyridine) were synthesized and purified according to the reported procedures. All reactions were performed under a nitrogen or an argon atmosphere (where noted). Column chromatography was performed using Kanto Chemical silica gel 60 N (spherical, neutral). Deionized water was freshly prepared from a water purification system (MILIPORE) and used throughout. The human female cervix tumor cell line, HeLa (RCB0007), was provided by the RIKEN BioResource Center.

Apparatus

Melting points were determined on a Yanaco melting point apparatus and not corrected. The ^{1}H NMR spectra were recorded on a Bruker AV400 spectrometer at 400 MHz. The ^{13}C NMR spectra were recorded on a Bruker AV400 spectrometer at 100 MHz. For the ^{1}H and ^{13}C NMR measurements, tetramethylsilane (TMS) was used as the internal standard. The pH was recorded using an MM-60R instrument (TDADKK). The UV-vis spectra were recorded on a JASCO V-660 spectrophotometer. The fluorescence spectra and absolute quantum yields were measured on a Hitachi F-4500 spectrometer and a Hamamatsu Photonics absolute PL quantum yield measurement system C9920-02, respectively. The ESI-TOF mass spectra were recorded on an Applied Biosystems QStar Pulsar *i* spectrometer and a Waters SYNAPT G2 system. Elemental analyses were performed at the Chemical Analysis Center, University of Tsukuba. All bright-field imaging and luminescence imaging measurements were carried out on an Olympus FV-1000 microscope. The luminophore in HeLa cells was excited with a high-pressure Hg lamp through a 460–490 nm filter, and emission was collected over 500 nm. The image processing was performed using the QCaptuer Pro 6.0 software.

Synthesis

ANMM-bpy: A mixture of 4-amino-3-nitrophenol (925 mg, 6.00 mmol) and NaH (144 mg, 6.00 mmol) was stirred in 60 mL of dry acetonitrile at room temperature under an argon atmosphere. After 15 min, a solution of **BM-bpy** (526 mg, 2.00 mmol) in 20 mL of dry acetonitrile was injected. The suspension was stirred overnight and then filtered to remove the precipitate. The filtrate was evaporated and purified by flash column chromatography (SiO_2; CH_2Cl_2–acetone, 10 : 1, v/v) to give **ANMM-bpy** as an orange powder. Yield: 74%, m.p. 202–205 °C. ^{1}H NMR (400 MHz, $CDCl_3$) δ (ppm): 8.69 (d, J = 5.2 Hz, 1H), 8.55 (d, J = 5.2 Hz, 1H), 8.46 (s, 1H), 8.26 (s, 1H), 7.65 (d, J = 2.8 Hz, 1H), 7.38 (d, J = 4.8 Hz, 1H), 7.19 (d, J = 9.2 Hz, 1H), 7.16 (d, J = 4.8 Hz, 1H), 6.79 (d, J = 9.2 Hz, 1H), 5.92 (s, 2H), 5.13 (s, 2H), 2.45 (s, 3H); ^{13}C NMR (100 MHz, $CDCl_3$) δ (ppm): 156.75, 155.61, 149.49, 149.33, 149.05, 148.26, 146.54, 140.29, 131.48, 126.98, 124.94, 122.11, 121.54, 120.27, 119.12, 108.16, 69.21, 21.21; positive-ion ESI-MS m/z calcd for $[C_{18}H_{17}N_4O_3]^+$ ($[M + H]^+$): 337.1, found: 337.0.

Ir-HM: A suspension of $[\mathbf{Ir(tpy)_2Cl}]_2$ (113 mg, 0.10 mmol) and **HM-bpy** (40 mg, 0.20 mmol) in CH_2Cl_2 and CH_3OH (30 mL, 1 : 1, v/v) was heated to reflux while stirring under a nitrogen atmosphere. After 12 h the resulting yellow solution was cooled to room temperature. The solution volume was then reduced to approximately 15 mL and ammonium hexafluorophosphate (5-fold excess, aq., 10 mL) was added. After stirring for 2 h, the mixture was evaporated and the residue was dissolved in CH_2Cl_2 (30 mL). The solution was washed

with water and brine and then dried over $MgSO_4$. After filtration, the solvent was removed under vacuum. The crude product was purified by column chromatography (SiO_2; CH_2Cl_2–acetone, 20 : 1, v/v) and **Ir-HM** was obtained as a yellow powder. Yield, 94%, m.p. 270–273 °C. ^{1}H NMR (400 MHz, CD_3CN) δ (ppm): 8.46 (s, 1H), 8.39 (s, 1H), 7.98 (d, J = 8.0 Hz, 2H), 7.88 (d, J = 5.6 Hz, 1H), 7.81–7.77 (m, 3H), 7.67 (d, J = 8.0 Hz, 2H), 7.54 (d, J = 6.0 Hz, 2H), 7.42 (d, J = 6.0 Hz, 1H), 7.31 (d, J = 5.6 Hz, 1H), 6.96 (d, J = 6.0 Hz, 2H), 6.86 (d, J = 8.0 Hz, 2H), 6.09 (s, 2H), 4.78 (d, J = 4.2 Hz, 2H), 3.72 (t, J = 5.6 Hz, 1H), 2.52 (s, 3H), 2.09 (s, 6H); ^{13}C NMR (100 MHz, CD_3CN) δ (ppm): 168.56, 156.71, 156.42, 152.87, 151.90, 151.86, 151.00, 150.73, 149.80, 142.36, 141.42, 139.20, 133.22, 129.87, 126.24, 126.10, 125.74, 124.31, 123.77, 122.23, 120.35, 62.61, 21.69, 21.36; positive-ion ESI-MS m/z calcd for $[C_{36}H_{32}IrN_4O]^+$ ($[M - PF_6]^+$): 729.2, found: 729.2; elemental analysis calcd (%) for $C_{36}H_{32}IrN_4OPF_6 \cdot H_2O$: C 48.48, H 3.84, N 6.28; found: C 48.67, H 3.98, N 5.96.

Ir-ANMM: A suspension of $[\mathbf{Ir(tpy)_2Cl}]_2$ (113 mg, 0.10 mmol) and **ANMM-bpy** (67 mg, 0.20 mmol) in CH_2Cl_2 and CH_3OH (30 mL, 1 : 1, v/v) was heated to reflux while stirring under a nitrogen atmosphere. After 12 h the resulting solution was cooled to room temperature. The solution volume was then reduced to approximately 15 mL and ammonium hexafluorophosphate (5-fold excess, aq., 10 mL) was added. After stirring for 2 h, the mixture was evaporated and the residue was dissolved in CH_2Cl_2 (30 mL). The solution was washed with water and brine and then dried over $MgSO_4$. After filtration, the solvent was removed under vacuum. The crude product was purified by column chromatography (SiO_2; CH_2Cl_2–acetone, 20 : 1, v/v) and **Ir-ANMM** was obtained as an orange powder. Yield, 96%, m.p. >300 °C. ^{1}H NMR (400 MHz, CD_3CN) δ (ppm): 8.56 (s, 1H), 8.42 (s, 1H), 7.98 (d, J = 7.6 Hz, 2H), 7.94 (d, J = 5.6 Hz, 1H), 7.82–7.77 (m, 3H), 7.67 (d, J = 7.6 Hz, 2H), 7.61 (d, J = 2.8 Hz, 1H), 7.54 (d, J = 5.6 Hz, 2H), 7.51 (dd, J = 5.6, 1.6 Hz, 1H), 7.33 (dd, J = 5.6, 1.6 Hz, 1H), 7.26 (dd, J = 9.2, 2.8 Hz, 1H), 6.98–6.94 (m, 3H), 6.86 (dd, J = 8.0, 1.2 Hz, 2H), 6.39 (s, 2H), 6.09 (d, J = 4.8 Hz, 2H), 5.24 (s, 2H), 2.54 (s, 3H), 2.09 (s, 6H); ^{13}C NMR (100 MHz, CD_3CN) δ (ppm): 168.55, 157.17, 156.21, 152.96, 151.72, 151.39, 151.20, 150.81, 149.82, 149.20, 142.70, 142.35, 141.49, 139.26, 133.19, 131.55, 130.06, 127.85, 126.75, 126.43, 125.77, 124.39, 123.80, 122.91, 121.61, 120.40, 109.18, 69.23, 21.71, 21.40; positive-ion ESI-MS m/z calcd for $[C_{42}H_{36}IrN_6O_3]^+$ ($[M - PF_6]^+$): 865.2, found: 865.3; elemental analysis calcd (%) for $C_{42}H_{36}IrN_6O_3PF_6 \cdot CH_2Cl_2 \cdot (CH_3)_2CO$: C 47.92, H 3.85, N 7.29; found: C 48.26, H 3.83, N 7.41.

General procedures for luminescent sensing experiments

Unless otherwise noted, all luminescent sensing measurements were carried out at room temperature in CH_3CN–0.1 M phosphate buffer (1 : 4, v/v, pH 7.4). Specifically, to a 5 mL volumetric flask, 0.1 mL of the stock solution (2.5×10^{-4} M) of **Ir-ANMM** in CH_3CN was added, followed by the addition of 0.9 mL CH_3CN and 2 mL phosphate buffer (0.1 M, pH 7.4). Then an appropriate volume of the ROS/RNS (see ESI†) was added, and the final volume was adjusted to 5 mL with phosphate buffer. All samples were allowed to stand at room temperature for at least 3 h before measurement. Luminescent spectra were obtained in 10 × 10 mm quartz cells with the excitation at 400 nm.

Luminescent imaging of HeLa cells

HeLa cells were seeded on glass-bottomed dishes and cultured in Dulbecco's modified Eagle's medium (DMEM) for 24 h at 37 °C in a 5% CO_2–95% air incubator. The concentrated stock solution of **Ir-ANMM** (1 mM) was prepared by dissolving **Ir-ANMM** in DMSO. Before cell loading, the cultured HeLa cells were washed twice and then incubated with **Ir-ANMM** (final concentration: 20 μM) in fresh cell culture medium. After incubation for 1 h at 37 °C in a 5% CO_2–95% air incubator, the cells were washed three times with fresh DMEM media and further incubated with or without HOCl (final concentration: 50 μM) for 0.5 h. The cells were rinsed three times with fresh DMEM before being subjected to luminescence microscopy imaging measurement.

Theoretical calculations

All the calculations based on the density functional theory (DFT) were carried out using the Gaussian 09 program package.[15] The hybrid Hartree Fock/density functional theory (HF/DFT) method B3LYP was utilized to optimize the geometry of the ground state. The "double-ζ" quality basis set consisting of Hay and Wadt's effective core potentials (LANL2DZ) was employed for the treatment of the iridium(III) atom, while the 6-31G* basis set was used for the treatment of the H, C, O and N atoms. A relativistic effective core potential (ECP) replaced the inner core electrons of Ir^{III}, leaving the outer core ($5s^25p^6$) electrons and the $5d^6$ valence electrons. Based on these optimizations, 40 ground-to-excited state singlet–singlet transition energies (20 for **Ir-HM**) and 3 excited state triplet transition energies were obtained to determine the vertical excitation energies of **Ir-ANMM** and **Ir-HM** using the time-dependent DFT (TD-DFT) calculations.

Results and discussion

Synthesis and characterization

The synthetic procedures of **Ir-ANMM** and **Ir-HM** are shown in Scheme S1.† 4-Bromomethyl-4′-methyl-2,2′-bipyridine (**BM-bpy**),[12] 4-hydroxymethyl-4′-methyl-2,2′-bipyridine (**HM-bpy**)[13] and $[\mathbf{Ir(pba)_2Cl}]_2$ [14] were synthesized and purified according to the reported procedures. The ligand 4-[(4-amino-3-nitrophenoxy)-methylene]-4′-methyl-2,2′-bipyridine (**ANMM-bpy**) was synthesized through the nucleophilic substitution of **BM-bpy** by 4-amino-3-nitrophenol in dry CH_3CN in the presence of NaH. The ligand was characterized by ^{1}H NMR, ^{13}C NMR and ESI-MS. The two complexes **Ir-ANMM** and **Ir-HM** were synthesized through the bridge splitting reaction of $[\mathbf{Ir(tpy)_2Cl}]_2$ and subsequent complexation with **ANMM-bpy** and **HM-bpy**, respectively. The complexes were both purified through

column chromatography, with **Ir-ANMM** isolated as an orange powder in 96% yield, while **Ir-HM** was isolated as a yellow powder in a yield of 94%. Both **Ir-ANMM** and **Ir-HM** were characterized by ^{1}H NMR, ^{13}C NMR, ESI-MS and elemental analysis.

Photophysical properties

The UV-vis absorption and photoluminescent spectra of **Ir-ANMM** and **Ir-HM** are shown in Fig. 1 and the photophysical data are summarized in Table S1.† In the electronic absorption spectra, both complexes exhibit intense absorption bands with extinction coefficients on the order of 10^4 dm^3 mol^{-1} cm^{-1} in the wavelength region shorter than 335 nm. These bands, by comparison with the absorption characteristics of related bis-cyclometalated iridium(III) diimine complexes,[16] can be ascribed to the ligand-centered (LC) (^{1}IL of π→π*(C^N) and ^{1}LLCT of π(C^N)→π*(N^N)) transitions. The less intense absorption bands in the 335–492 nm (335–444 nm for **Ir-HM**) region with extinction coefficients on the order of 10^3 dm^3 mol^{-1} cm^{-1} are assigned to a mixture of the spin-allowed metal-to-ligand charge-transfer (^{1}MLCT) (dπ(Ir)→π*(C^N and N^N)) transitions and ligand-to-ligand charge-transfer (^{1}LLCT) (π(C^N)→π*(N^N)) transitions. Such an ascription is further confirmed by the TD-DFT calculations (*vide infra*).

As recorded in Table S1,† in aerobic acetonitrile, **Ir-ANMM** and **Ir-HM** both exhibited weak emission with low quantum yields of 0.01 and 0.04, respectively. In contrast, under anaerobic conditions, weak emission of **Ir-ANMM** (λ_{em}^{max} = 619 nm, Φ_{em} = 0.02) and efficient yellow emission of **Ir-HM** (λ_{em}^{max} = 611 nm, Φ_{em} = 0.17) were observed. The extremely weak emission of **Ir-ANMM** confirmed the efficient PET effect imposed by the electron-rich 4-amino-3-nitrophenyl moiety. The highly oxygen-sensitive quantum yields suggested that the emission arises from a triplet state. Moreover, the emission bands of both **Ir-ANMM** and **Ir-HM** are dependent on the solvent polarity (Fig. S1†), suggesting the ^{3}MLCT (dπ(Ir)→π*(bpy and C^N)) dominated excited states of the complexes,[17] which was further verified by the TD-DFT calculation studies.

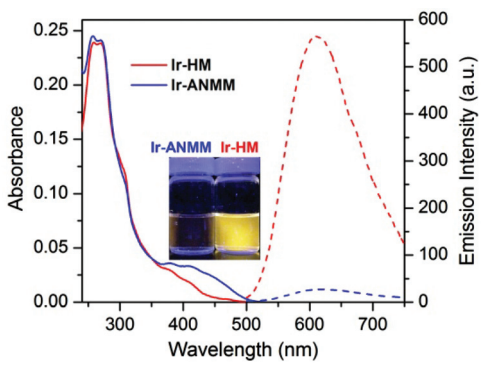

Fig. 1 The UV-vis absorption (solid lines) and PL emission (dash lines) spectra of **Ir-ANMM** (5 μM) (blue) and **Ir-HM** (5 μM) (red). CH_3CN. λ_{ex} = 400 nm. Inset: emission photographs of **Ir-ANMM** and **Ir-HM**.

DFT calculations

The TD-DFT calculations were carried out to acquire the relevant transition energies of **Ir-ANMM** and **Ir-HM**, aiming for a complete apprehension of the photophysical properties of both complexes. The optimized structures of **Ir-ANMM** and **Ir-HM** in the ground states are shown in Fig. S2,† based on which the absorption transitions of both complexes have been calculated. Fig. S3† shows an excellent accordance of the calculated absorption transitions of **Ir-ANMM** and **Ir-HM** with their experimental spectra, confirming the applicable description of these complexes by this calculation level. Additionally, the calculated results in Tables S2 and S4† agree well with the former ascription of the intense absorption bands below 335 nm predominantly to LC (**Ir-ANMM**: S30, S38, S39; **Ir-HM**: S15, S17, S20) transitions and the absorption bands above 335 nm to an admixture of ^{1}LLCT–^{1}MLCT (**Ir-ANMM**: S2, S8, S9, S10; **Ir-HM**: S2, S4, S7, S9) transitions.

According to Table 1, the lowest triplet (T1) states of **Ir-ANMM** and **Ir-HM** both originate from the HOMO–LUMO (**Ir-ANMM**: 98.0%; **Ir-HM**: 98.2%) transitions. As shown in Table 2, Tables S3 and S5,† the calculated HOMO of both complexes mainly resides on the iridium center (**Ir-ANMM**: 41.8%; **Ir-HM**: 42.0%) and the LUMO of both are dominantly located on the bipyridine ligand (**Ir-ANMM**: 91.1%; **Ir-HM**: 94.5%). Accordingly, both HOMO–LUMO transitions of **Ir-ANMM** and **Ir-HM** are predominantly assigned to the ^{3}MLCT (dπ(Ir)→π*-(bpy)) characteristics, which are consistent with the previous attribution. With similar MLCT units though, **Ir-ANMM** exhibits a much lower emission quantum yield than **Ir-HM**, which should originate from the PET effect imposed by its electron-rich 4-amino-3-nitrophenyl moiety.[10]

Optimization of sensing conditions

To explore the possibility of sensing HOCl in aqueous media, the effect of water on the emission of **Ir-ANMM** and **Ir-HM** was investigated. As shown in Fig. S6,† introduction of various amounts of water exerted very small effects on the luminescence of **Ir-ANMM**, with constantly weak emission in diverse solvent systems. Similarly, small amounts of water also have little influence on the emission of the complex **Ir-HM**, leading to a slight enhancement of its emission intensity. However, with a large ratio of water, over 90% in particular, the emission intensity dramatically reduced, which is definitely a serious disadvantage since the distinct emission intensity gap of **Ir-ANMM** and **Ir-HM** is necessary for the sensitive detection of HOCl in such an emission turn-on sensing system. Taking into account the disadvantageous influence of a large amount of water on the emission of **Ir-HM** and the significance of detecting analytes in aqueous media, CH_3CN–H_2O (1 : 4, v/v) was chosen as an appropriate solvent system for the sensing of HOCl.

The appropriate water solubility makes the sensor promising for intracellular applications. Accordingly, the applicability of the sensor to biological systems was explored by studying the influence of pH on the emission of **Ir-ANMM** and **Ir-HM**.

Table 1 Calculated excited states of **Ir-ANMM** and **Ir-HM**

Complex	State	Transition	Contri.	*E*/nm (eV)	Assignment
Ir-ANMM	T1	HOMO → LUMO	98.0%	612 (2.02)	^{3}MLCT/^{3}LLCT
Ir-HM	T1	HOMO → LUMO	98.2%	593 (2.09)	^{3}MLCT/^{3}LLCT

Table 2 Calculated molecular orbitals of **Ir-ANMM** and **Ir-HM**

	Ir-ANMM	**Ir-HM**
LUMO	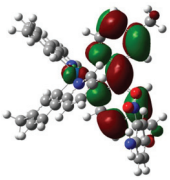	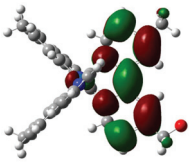
HOMO	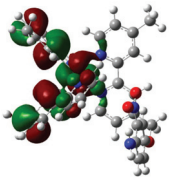	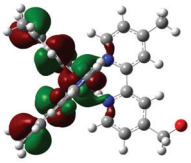

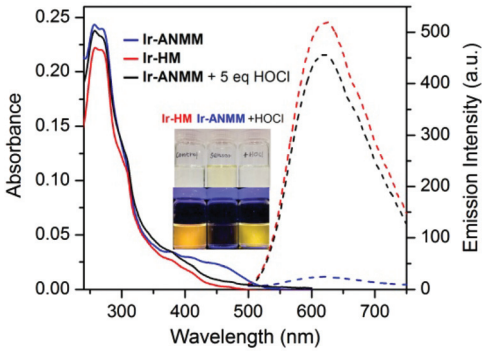

Fig. 2 The UV-vis absorption (solid lines) and PL emission (dash lines) spectra of **Ir-HM** (5 μM) (red), **Ir-ANMM** (5 μM) in the absence (blue) and presence (black) of 5 equiv. of HOCl. CH_3CN–0.1 M phosphate buffer (1 : 4, v/v, pH 7.4). λ_{ex} = 400 nm. Inset: photographs of the color (top) and PL emission (bottom) of **Ir-HM** (20 μM) and **Ir-ANMM** (20 μM) before and after the addition of 5 equiv. of HOCl.

As shown in Fig. S7,† pH has negligible influence on the emission of both complexes in a range from pH 4.5 to pH 10.5, indicating that the sensor is suitable for use under physiological conditions. Based on these results, pH 7.4 was selected for all the sensing experiments.

Typically, for a chemodosimeter, a fast response is a very important factor for practical applications. Therefore, the effect of time on **Ir-ANMM** sensing of HOCl was investigated under the above optimized conditions, *i.e.* in a CH_3CN–0.1 M phosphate buffer (1 : 4, v/v, pH 7.4) solvent system. As shown in Fig. S8,† the emission intensity of **Ir-ANMM** was dramatically enhanced immediately after the addition of 5 equiv. of HOCl, suggesting the feasibility of HOCl sensing by **Ir-ANMM** in the solvent system. Significantly, the reaction reached completion within 20 min as monitored by the emission intensity changes, indicating a relatively fast response of **Ir-ANMM** toward HOCl.

To ensure thorough reaction, all samples were measured after standing at room temperature for at least 3 hours for all the sensing experiments.

Optical response of Ir-ANMM to HOCl

The photophysical responses of **Ir-ANMM** toward HOCl under the optimized conditions are shown in Fig. 2. With higher absorbance in the visible range, the solution of **Ir-ANMM** was pale yellow. In the presence of HOCl, however, the absorbance in the visible range decreased and the solution color became colorless.

The luminescence exhibits a much more pronounced response. In the absence of HOCl, **Ir-ANMM** showed very weak emission. Nevertheless, in the presence of HOCl, the emission intensity was enhanced dramatically and the solution emitted strong yellow light. The absorption and emission spectra, solution color and emission color of the **Ir-ANMM**–HOCl mixture were all very similar to those of **Ir-HM**, strongly implying the HOCl-promoted oxidation of **Ir-ANMM** to generate **Ir-HM** in this solvent system.

In addition to the optical spectral changes, ^{1}H NMR spectroscopy was also employed to provide direct evidence of the assumed sensing mechanism. As shown in Fig. S9,† in the presence of HOCl, the ^{1}H NMR spectrum of **Ir-ANMM** changed strikingly. The disappearance of $H_{6''}$ and $H_{4''}$ indicated the cleavage of the 4-amino-3-nitrophenyloxy moiety. The upfield shifts of H_3, H_5, H_6, H_j and the spectral similarity to that of **Ir-HM** have unambiguously confirmed the production of **Ir-HM** from the reaction between **Ir-ANMM** and HOCl.

Moreover, the mechanism was further confirmed by ESI-MS spectral changes. As shown in Fig. S10a,† the chemodosimeter **Ir-ANMM** showed a featured *m*/*z* peak of [**Ir-ANMM** – PF_6]$^+$ at 865.3. However, the peak disappeared in the presence of 4 equiv. of HOCl (Fig. S10b†), with the appearance of a new *m*/*z* peak at 729.2 characteristic of [**Ir-HM** – PF_6]$^+$ (Fig. S10c†). All these results strongly demonstrated the HOCl-promoted oxidation reaction of **Ir-ANMM** to generate **Ir-HM**.

Sensitive response of Ir-ANMM to HOCl

The detailed luminescent response of **Ir-ANMM** toward HOCl has been carefully investigated by phosphorescence emission spectroscopies. As shown in Fig. 3a, in the absence of HOCl, **Ir-ANMM** exhibits very weak emission. However, upon treatment with an increasing concentration of HOCl, the weak

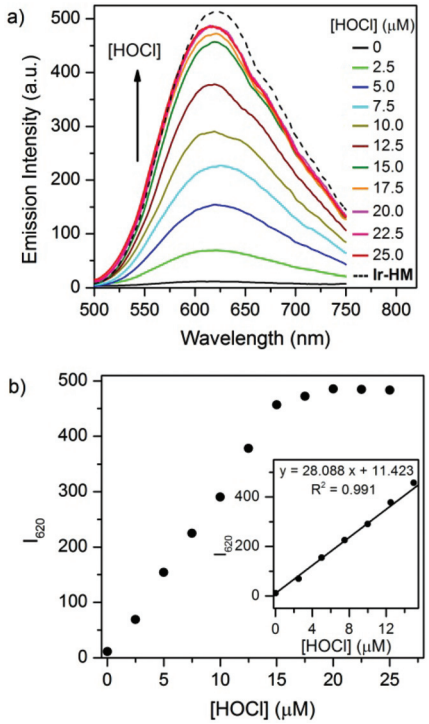

Fig. 3 (a) The luminescent spectral changes of **Ir-ANMM** (5 μM) upon increasing addition of HOCl (from 0.0 to 25.0 μM). CH_3CN–0.1 M phosphate buffer (1 : 4, v/v, pH 7.4). λ_{ex} = 400 nm. (b) The emission intensity I_{620} *vs.* the concentration of HOCl; inset: the linear relation of I_{620} *vs.* the concentration of HOCl in the range of 0.0–15.0 μM.

emission was gradually enhanced and reached saturation when 4 equiv. of HOCl was added. The titration curve was depicted in Fig. 3b in which the emission intensity I_{620} increased in proportion to the HOCl concentration. Interestingly, the emission intensity I_{620} showed an excellent linear relationship with the HOCl concentration in the range of 0 to 15 μM (inset of Fig. 3b), indicating the feasibility of **Ir-ANMM** for the quantitative determination of the HOCl concentration. The detection limit, calculated from the linear equation, is 16 nM at the signal to noise ratio (S/N) = 3, which is much lower than many reported luminescent HOCl sensors[18] and therefore confirms the highly sensitive response of **Ir-ANMM** to HOCl.

Selective response of Ir-ANMM to HOCl among various ROS/RNS

The specific response of **Ir-ANMM** to HOCl was verified through examination of the emission spectroscopic changes of **Ir-ANMM** upon the addition of various ROS/RNS including H_2O_2, $^{\bullet}OH$, $^1O_2$, $O_2^{-\bullet}$, ^{t}BuOOH, $ROO^{\bullet}$, $NO^{\bullet}$, NO_2^-, NO_3^- and $ONOO^-$. As shown in Fig. S11,† **Ir-ANMM** exhibited a remarkable emission enhancement only in the presence of HOCl. Conversely, in the presence of other ROS/RNS, even with a large excess, negligible or only slight variations of the emission spectra could be observed. The selectivity toward HOCl was assessed by the emission intensity I_{620} changes. As shown in Fig. 4, HOCl led to a 38-fold increase of the emission intensity

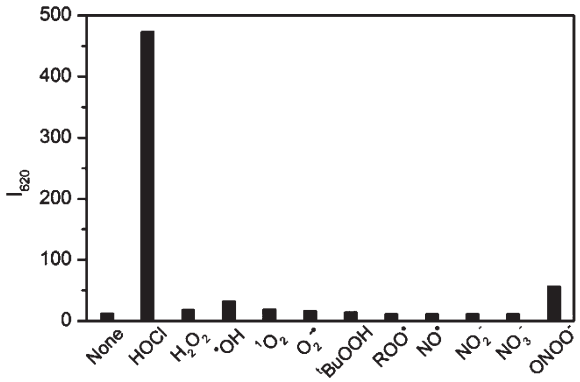

Fig. 4 Emission intensity I_{620} of **Ir-ANMM** (5 μM) in the presence of various ROS/RNS. HOCl (25 μM), $ONOO^-$ (50 μM), and other (200 μM). CH_3CN–0.1 M phosphate buffer (1 : 4, v/v, pH 7.4). λ_{ex} = 400 nm.

I_{620}, while $ONOO^-$ resulted in a 4.5-fold enhancement and all the other species generated negligible emission enhancement (<2.6-fold). These results clearly demonstrated the high specificity of **Ir-ANMM** toward HOCl. Such a superior selectivity for HOCl was attributed to the strong oxidizing capability of HOCl, which could promote the oxidation of the *o*-nitroanilino group in **Ir-ANMM**.

Intracellular imaging of HOCl

The feasibility of the sensor under physiological conditions, the high selectivity and the high sensitivity strongly supported the examination of the applicability of **Ir-ANMM** for the determination of HOCl in living cells. Therefore, the feasibility of **Ir-ANMM** for imaging HOCl in HeLa cells was evaluated. As shown in Fig. 5a, the **Ir-ANMM**-loaded cells exhibit negligible intracellular luminescence. In sharp contrast, the **Ir-ANMM**-loaded cells further incubated with HOCl resulted in a remarkable enhancement of the red intracellular luminescence (Fig. 5b). These results indicated that **Ir-ANMM** was cell membrane permeable and capable of interacting with HOCl to generate measurable luminescent signals in the living cells.

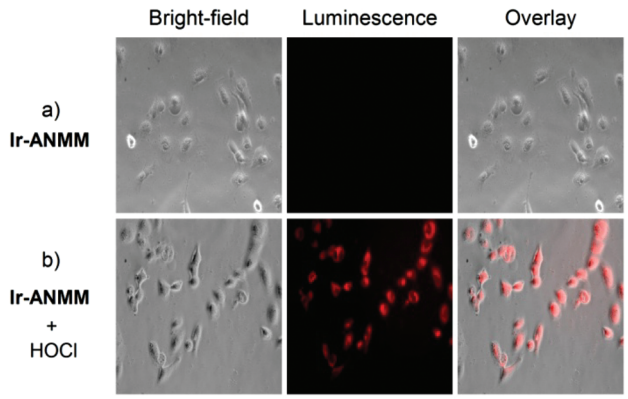

Fig. 5 Images of HOCl in HeLa cells. (a) Images of the cells incubated with **Ir-ANMM** (20 μM) only. (b) Images of **Ir-ANMM**-loaded cells after treatment with HOCl (50 μM).

Conclusions

A novel and easily accessible phosphorescent biscyclometalated iridium(III) complex **Ir-ANMM** exhibiting a turn-on luminescent response to HOCl in aqueous media has been synthesized and characterized. Upon the addition of HOCl, the electron-rich PET-quenching 4-amino-3-nitrophenyl moiety of the non-luminescent **Ir-ANMM** was cleaved, giving rise to a new highly luminescent complex **Ir-HM**. The remarkable emission enhancement is accordingly able to indicate HOCl. Through luminescent titration experiments, the limit of detection was determined to be as low as 16 nM. Moreover, the specific reaction makes the chemodosimeter **Ir-ANMM** highly selective for HOCl among various ROS/RNS. With appropriate water solubility, low detection limit and high selectivity, the probe was successfully employed for living cell imaging of HOCl, making it a very promising tool for intracellular HOCl sensing.

Acknowledgements

This research was financially supported by Grants-in-Aid for Scientific Research from the Ministry of Education, Culture, Sports, Science, and Technology of Japan.

Notes and references

1 (*a*) W. A. Rutala and D. J. Weber, *Clin. Microbiol. Rev.*, 1997, **10**, 4597; (*b*) S. Fukuzaki, *Biocontrol Sci.*, 2006, **11**, 147; (*c*) M. A. Shannon, P. W. Bohn, M. Elimelech, J. G. Georgiadis, B. J. Marinas and A. M. Mayes, *Nature*, 2008, **452**, 301.

2 (*a*) C. M. Spickett, A. Jerlich, O. M. Panasenko, J. Arnhold, A. R. Pitt, T. Stelmaszyñska and R. J. Schaur, *Acta Biochim. Pol.*, 2000, **47**, 889; (*b*) W. A. Prütz, *Arch. Biochem. Biophys.*, 1996, **332**, 110; (*c*) M. Sabine, H. Ulrike, S. Wolfgang, W. Jian, A. Jürgen, P. Kostas and M. Sebastian, *J. Biol. Chem.*, 2003, **278**, 40542; (*d*) C. Bergt, S. Pennathur, X. Fu, J. Byun, K. O'Brien, T. O. McDonald, P. Singh, G. M. Anantharamaiah, A. Chait, J. Brunzell, R. L. Geary, J. F. Oram and J. W. Heinecke, *Proc. Natl. Acad. Sci. U. S. A.*, 2004, **101**, 13032.

3 (*a*) G. L. Squadrito, E. M. Postlethwait and S. Matalon, *Am. J. Physiol.*, 2010, **299**, L289; (*b*) M. J. Davies, C. L. Hawkins, D. I. Pattison and M. D. Rees, *Antioxid. Redox Signaling*, 2008, **10**, 1199; (*c*) G. Dever, C. P. Oliveira, L. J. Stewart and C. M. Spickett, *Free Radical Res.*, 2003, **37**, 27; (*d*) I. B. Zavodnik, E. A. Lapshina, L. B. Zavodnik, M. Soszyński, G. Bartosz and M. Bryszewska, *Bioelectrochemistry*, 2002, **58**, 127; (*e*) J. M. Pullar, M. C. M. Vissers and C. C. Winterbourn, *IUBMB Life*, 2000, **50**, 259.

4 (*a*) M. Emrullahoglu, M. Ucuncu and E. Karakus, *Chem. Commun.*, 2013, **49**, 7836; (*b*) L. Yuan, W. Lin, Y. Xie, B. Chen and J. Song, *Chem. – Eur. J.*, 2012, **18**, 2700; (*c*) Y. Koide, Y. Urano, K. Hanaoka, T. Terai and T. Nagano, *J. Am. Chem. Soc.*, 2011, **133**, 5680; (*d*) S.-R. Liu and S.-P. Wu, *Org. Lett.*, 2013, **15**, 878.

5 V. Fernandez-Moreira, F. L. Thorp-Greenwood and M. P. Coogan, *Chem. Commun.*, 2010, **46**, 186.

6 (*a*) M. S. Lowry and S. Bernhard, *Chem. – Eur. J.*, 2006, **12**, 7970; (*b*) C. Ulbricht, B. Beyer, C. Friebe, A. Winter and U. S. Schubert, *Adv. Mater.*, 2009, **21**, 4418; (*c*) P. A. Vigato, V. Peruzzo and S. Tamburini, *Coord. Chem. Rev.*, 2009, **253**, 1099; (*d*) Y. Chi and P.-T. Chou, *Chem. Soc. Rev.*, 2010, **39**, 638; (*e*) Q. Zhao, C. Huang and F. Li, *Chem. Soc. Rev.*, 2011, **40**, 2508; (*f*) S.-J. Liu, Y. Chen, W.-J. Xu, Q. Zhao and W. Huang, *Macromol. Rapid Commun.*, 2012, **33**, 461; (*g*) K. K.-W. Lo, A. W.-T. Choi and W. H.-T. Law, *Dalton Trans.*, 2012, **41**, 6021.

7 (*a*) Q. Zhao, F. Li and C. Huang, *Chem. Soc. Rev.*, 2010, **39**, 3007; (*b*) V. Guerchais and J.-L. Fillaut, *Coord. Chem. Rev.*, 2011, **255**, 2448; (*c*) K. K.-W. Lo, S. P.-Y. Li and K. Y. Zhang, *New J. Chem.*, 2011, **35**, 265.

8 N. Zhao, Y.-H. Wu, R.-M. Wang, L.-X. Shi and Z.-N. Chen, *Analyst*, 2011, **136**, 2277.

9 F. B. Mallory, *Org. Synth.*, 1957, **37**, 1.

10 Y. Xiao, R. Zhang, Z. Ye, Z. Dai, H. An and J. Yuan, *Anal. Chem.*, 2012, **84**, 10785.

11 (*a*) D.-G. Cho and J. L. Sessler, *Chem. Soc. Rev.*, 2009, **38**, 1647; (*b*) J. Du, M. Hu, J. Fan and X. Peng, *Chem. Soc. Rev.*, 2012, **41**, 4511; (*c*) K. Kaur, R. Saini, A. Kumar, V. Luxami, N. Kaur, P. Singh and S. Kumar, *Coord. Chem. Rev.*, 2012, **256**, 1992.

12 J. Gu, J. Chen and R. H. Schmehl, *J. Am. Chem. Soc.*, 2010, **132**, 7338.

13 A. T. Dickschat, F. Behrends, S. Surmiak, M. Weiß, H. Eckert and A. Studer, *Chem. Commun.*, 2013, **49**, 2195.

14 (*a*) M. Nonoyama, *Bull. Chem. Soc. Jpn.*, 1974, **47**, 767; (*b*) S. Sprouse, K. A. King, P. J. Spellane and R. J. Watts, *J. Am. Chem. Soc.*, 1984, **106**, 6647; (*c*) J. C. Freys, G. Bernardinelli and O. S. Wenger, *Chem. Commun.*, 2008, 4267.

15 M. J. Frisch, G. W. Trucks, H. B. Schlegel, G. E. Scuseria, M. A. Robb, J. R. Cheeseman, G. Scalmani, V. Barone, B. Mennucci, G. A. Petersson, H. Nakatsuji, M. Caricato, X. Li, H. P. Hratchian, A. F. Izmaylov, J. Bloino, G. Zheng, J. L. Sonnenberg, M. Hada, M. Ehara, K. Toyota, R. Fukuda, J. Hasegawa, M. Ishida, T. Nakajima, Y. Honda, O. Kitao, H. Nakai, T. Vreven, J. A. Montgomery Jr., J. E. Peralta, F. Ogliaro, M. Bearpark, J. J. Heyd, E. Brothers, K. N. Kudin, V. N. Staroverov, T. Keith, R. Kobayashi, J. Normand, K. Raghavachari, A. Rendell, J. C. Burant, S. S. Iyengar, J. Tomasi, M. Cossi, N. Rega, J. M. Millam, M. Klene, J. E. Knox, J. B. Cross, V. Bakken, C. Adamo, J. Jaramillo, R. Gomperts, R. E. Stratmann, O. Yazyev, A. J. Austin, R. Cammi, C. Pomelli, J. W. Ochterski, R. L. Martin, K. Morokuma, V. G. Zakrzewski, G. A. Voth, P. Salvador, J. J. Dannenberg, S. Dapprich, A. D. Daniels, O. Farkas, J. B. Foresman, J. V. Ortiz, J. Cioslowski and

D. J. Fox, *GAUSSIAN 09 (Revision B. 01)*, Gaussian, Inc., Wallingford, CT, 2010.

16 (*a*) K. K.-W. Lo, C.-K. Chung and N. Zhu, *Chem. – Eur. J.*, 2003, **9**, 475; (*b*) K. K.-W. Lo, J. S.-Y. Lau, D. K.-K. Lo and L. T.-L. Lo, *Eur. J. Inorg. Chem.*, 2006, **2006**, 4054; (*c*) K. K.-W. Lo, C.-K. Chung, T. K.-M. Lee, L.-H. Lui, K. H.-K. Tsang and N. Zhu, *Inorg. Chem.*, 2003, **42**, 6886; (*d*) F. Lu, M. Yamamura and T. Nabeshima, *Tetrahedron Lett.*, 2013, **54**, 779; (*e*) F. Lu, M. Yamamura and T. Nabeshima, *Dalton Trans.*, 2013, **42**, 12093.

17 (*a*) Y. You and S. Y. Park, *Dalton Trans.*, 2009, 1267; (*b*) Q. Zhao, F. Li, S. Liu, M. Yu, Z. Liu, T. Yi and C. Huang, *Inorg. Chem.*, 2008, **47**, 9256.

18 (*a*) S. Chen, J. Lu, C. Sun and H. Ma, *Analyst*, 2010, **135**, 577; (*b*) G. Cheng, J. Fan, W. Sun, J. Cao, C. Hu and X. Peng, *Chem. Commun.*, 2014, **50**, 1018; (*c*) L. Yuan, W. Lin, J. Song and Y. Yang, *Chem. Commun.*, 2011, **47**, 12691; (*d*) Q. Xu, K.-A. Lee, S. Lee, K. M. Lee, W.-J. Lee and J. Yoon, *J. Am. Chem. Soc.*, 2013, **135**, 9944.